

SN2002ES-LIKE SUPERNOVAE FROM DIFFERENT VIEWING ANGLES

YI CAO¹, S. R. KULKARNI¹, AVISHAY GAL-YAM², S. PAPADOGIANNAKIS³, P. E. NUGENT^{4,5}, FRANK J. MASCI⁶,
BRIAN D. BUE⁷

Draft version January 20, 2021

ABSTRACT

In this letter, we compare optical light curves of two SN2002es-like Type Ia supernovae, iPTF14atg and iPTF14dpk, from the intermediate Palomar Transient Factory. Although the two light curves resemble each other around and after maximum, they show distinct early-phase rise behavior in the r -band. On the one hand, iPTF14atg revealed a slow and steady rise which lasted for 22 days with a mean rise rate of $0.2 \sim 0.3 \text{ mag day}^{-1}$, before it reached the R -band peak (-18.05 mag). On the other hand, iPTF14dpk rose rapidly to -17 mag within a day of discovery with a rise rate $> 1.8 \text{ mag day}^{-1}$, and then rose slowly to its peak (-18.19 mag) with a rise rate similar to iPTF14atg. The apparent total rise time of iPTF14dpk is therefore only 16 days. We show that emission from iPTF14atg before -17 days with respect to its maximum can be entirely attributed to radiation produced by collision between the SN and its companion star. Such emission is absent in iPTF14dpk probably because of an unfavored viewing angle, provided that SN2002es-like events arise from the same progenitor channel. We further show that a SN2002es-like SN may experience a dark phase after the explosion but before its radioactively powered light curve becomes visible. This dark phase may be hidden by radiation from supernova-companion interaction.

Subject headings: supernovae: general – supernovae: individual (SN2002es, iPTF14atg, iPTF14dpk)

1. INTRODUCTION

Type Ia supernovae (SNe Ia) are explosions of carbon-oxygen white dwarfs (WDs). There are two leading scenarios about their origins. In the single degenerate (SD) channel, WDs accrete mass from non-degenerate companion stars and explode when their masses approach the Chandrasekhar mass limit. In the double degenerate (DD) channel, merging or collision of WD pairs in binary or triple systems triggers the SN explosions (See Maoz et al. 2014 for a recent review).

There are multiple subclasses of Type Ia SNe: Branch-normal, SN1991T, super-Chandrasekhar, SN1991bg, Iax, SN2002es, etc.. The Type Iax (Foley et al. 2013) and SN2002es-like (Ganeshalingam et al. 2012) subclasses have low expansion velocities. Type Iax SNe lack Ti II absorption lines in their spectra and favor young stellar populations, whereas SN2002es-like events show prominent Ti II troughs and are associated with old stellar population (White et al. 2015). Both low-velocity SNe are possibly pure deflagration of WDs. Their low expansion velocities and large amount of intermediate mass elements are consistent with incomplete subsonic burning of carbon and oxygen (e.g., Fink et al. 2014). Recent

observations appear to find direct evidence for companion stars of two Type Iax SNe (McCully et al. 2014; Foley et al. 2014) and a SN2002es-like SN (Cao et al. 2015).

Following the discovery of a strong and declining UV pulse from a SN2002es-like supernova (SN) iPTF14atg within four days of explosion (Cao et al. 2015), it becomes particularly interesting to examine the early-phase light curve of other SN2002es-like events. If the UV pulse in iPTF14atg indeed arises from collision between the SN ejected material and a companion star, due to the viewing angle effect, it should be invisible in most of other SN2002es-like events.

Thanks to nightly-cadence surveys conducted as part of the intermediate Palomar Transient Factory (iPTF; Rau et al. 2009; Law et al. 2009), we found two SN2002es-like events between 2013 and 2015, internally designated as iPTF14atg and iPTF14dpk. Both events have well-sampled optical light curves and spectroscopic coverage. In this letter, we present the early-phase rise behavior of these two events.

The letter is organized as follows: In §2 we establish their similarities to SN2002es. In §3 we present the different rise behavior of the two events and seek an explanation. We conclude in §4.

2. SIMILARITY OF THE TWO EVENTS

Observations of iPTF14atg and iPTF14dpk were undertaken in the Mould R filter with the 48-inch Schmidt telescope at Palomar Observatory. Their light curves are produced by the PTF-IPAC forced photometry pipeline (Masci et al. in prep.) which uses pre-SN reference images to subtract off the host galaxy light, and performs point-spread function photometry at the location of a transient on the difference images. All magnitudes in this paper are in the AB system and calibrated to the PTF-IPAC catalog (Ofek et al. 2012b).

¹ Astronomy Department, California Institute of Technology, Pasadena, CA 91125, USA

² Department of Particle Physics and Astrophysics, Weizmann Institute of Science, Rehovot 76100, Israel

³ The Oskar Klein Centre, Department of Physics, Stockholm University, SE-106 91 Stockholm, Sweden

⁴ Department of Astronomy, University of California, Berkeley, CA 94720-3411, USA

⁵ Lawrence Berkeley National Laboratory, 1 Cyclotron Road, MS 50B-4206, Berkeley, CA 94720, USA

⁶ Infrared Processing and Analysis Center, California Institute of Technology, Pasadena, CA 91125, USA

⁷ Jet Propulsion Laboratory, California Institute of Technology, Pasadena, CA 91125, USA

Table 1
Two SN2002es-like Events in iPTF

Name	Coordinate (J2000)	Redshift	μ^a	Host Type	$E(B - V)^b$	Peak MJD ^c	Peak Mag. ^c
iPTF14atg	12 ^h 52 ^m 44.84 ^s +26°28′13.0″	0.0213	34.92	E-S0	0.011	56802.1	−18.05 ± 0.02
iPTF14dpk	16 ^h 45 ^m 19.35 ^s +40°09′41.3″	0.0387	36.23	Starburst	0.012	56878.1	−18.19 ± 0.02

^a The distance moduli μ are calculated with $H = 67.77 \text{ km s}^{-1} \text{ Mpc}^{-1}$ (Planck Collaboration et al. 2014). No redshift-independent distance measurement is available for the host galaxies of these events on the NASA/IPAC Extragalactic Database (NED).

^b The Galactic extinction map is given by Schlafly & Finkbeiner (2011).

^c The peak modified Julian dates (MJD) and magnitudes are measured from the PTF R -band light curves. The peak magnitudes do not include uncertainties from μ .

The spectra of iPTF14atg were published in Cao et al. (2015). The spectra of iPTF14dpk were obtained at -10 days with respect to its peak with the double spectrograph (DBSP; Oke & Gunn 1982) on the Palomar 200-inch Hale telescope, and at $+20$ and $+50$ days with the Low-Resolution Imaging Spectrometer (LRIS; Oke et al. 1995) on the Keck-I telescope at Mauna Kea. The spectra were reduced using standard IRAF/IDL routines. The spectra are made public through WISerEP (Yaron & Gal-Yam 2012).

In order to correct for the Galactic extinction, we use the Fitzpatrick (1999) model assuming $R_V = 3.1$. Regarding the host galaxy extinction, since the equivalent widths of Na I D absorption lines are correlated with the local extinction (Poznanski et al. 2012), the absence of Na I D absorption at the host galaxy redshifts in the spectra suggests that neither iPTF14atg nor iPTF14dpk is embedded in a dusty circumstellar medium. In fact, using the highest signal-to-noise ratio spectra of iPTF14atg and iPTF14dpk, assuming the width of the Na I D doublet is 200 km s^{-1} , we derived 3σ upper limits on the equivalent width of the doublet: $< 0.20 \text{ \AA}$ for iPTF14atg and $< 0.75 \text{ \AA}$ for iPTF14dpk. According to the empirical relation in Poznanski et al. (2012), these upper limits on the equivalent width corresponds to $E(B - V) < 0.02$ and $E(B - V) < 0.11$, respectively. In the following analysis, we do not correct for local extinction.

The primary data of the two events are summarized in Table 1. Their light curves and spectra are shown in Figures 1 and 2, respectively.

Next, in order to determine their peak magnitudes and dates, we use Gaussian process regression to interpolate the light curves (Figure 1). A squared exponential function is chosen as the autocorrelation function and the autocorrelation length is determined by the maximum likelihood estimation based on available data. Thanks to the almost nightly photometric sampling, the regression analysis determines both the peak dates and magnitudes with small uncertainties, as shown in Table 1.

We calculate k -correction in the Mould R -band for these two SNe using their spectra. We find that the k -correction is $\lesssim 0.2$ mag. Hence, going forward, we neglect the k -correction.

As shown in Figure 1, apart from the first few days after explosions, the light curves of both iPTF14atg and iPTF14dpk are quite similar. Since the Mould R filter is similar to the SDSS r filter (Ofek et al. 2012a), light curves of both iPTF14atg and iPTF14dpk also resemble the r -band light curve of SN2002es around maximum, though iPTF14atg does not show the fast decline

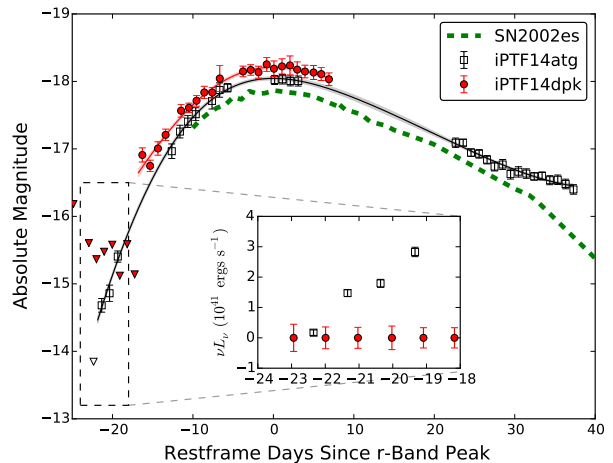


Figure 1. Light curves of iPTF14atg and iPTF14dpk. Black empty squares are iPTF14atg and red filled stars denote iPTF14dpk. Detection upper limits ($5\text{-}\sigma$) of pre-SN non-detections for iPTF14atg and iPTF14dpk are denoted by black empty and red filled downward triangles, respectively. The best interpolated light curves of iPTF14atg and iPTF14dpk with uncertainties from the Gaussian process regression are shown in red and black curves, respectively. For comparison, the green dashed curve shows the r -band light curve of SN2002es. The inset zooms in on the early-phase light curves of iPTF14atg and iPTF14dpk in the νL_ν space. The error bars represent 1σ uncertainties of each measurements (instead of 5σ upper limits in circumstances of null detection in the magnitude space).

seen in SN2002es after $t \simeq 30$ days. The peak magnitudes of iPTF14atg ($R = -18.05$ mag), iPTF14dpk ($R = -18.19$ mag) and SN2002es ($r = -18.35$ mag) are also comparable within the slight filter difference.

As can be seen in Figure 2, the spectra of iPTF14atg and iPTF14dpk around and after maxima also match those of SN2002es at similar phases. In particular, both iPTF14atg and iPTF14dpk show the low-velocity absorption lines and Ti II troughs, hallmark of SN2002es-like SNe. Next, the spectra of iPTF14atg and iPTF14dpk taken at -10 days share broad absorption features, although the continuum emission of iPTF14dpk appears bluer than that of iPTF14atg. This color difference might be due to residuals from imperfect subtraction of galaxy light in the spectra of iPTF14dpk, as iPTF14dpk is located close to the center of its apparently blue and compact host galaxy in an interacting galaxy pair. Therefore, we do not think that the blueness of the iPTF14atg indicates significant difference from iPTF14dpk.

Integrating the spectra and calibrating to the broad-

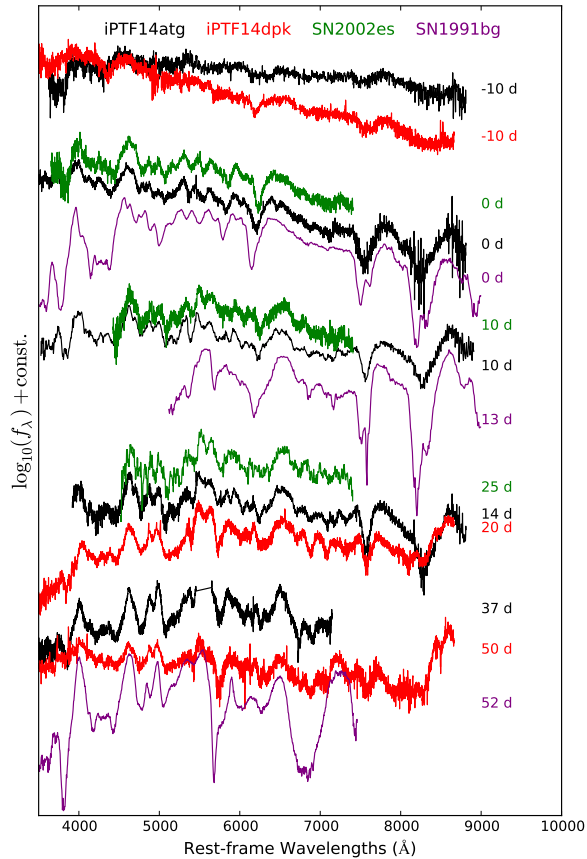


Figure 2. Spectral sequences of iPTF14atg and iPTF14dpk. The iPTF14atg spectra are taken from Cao et al. (2015) and shown in black while the iPTF14dpk spectra are in red. For comparison, we also show spectra of SN2002es (green; Ganeshalingam et al. 2012) and SN1991bg (purple, Filippenko et al. 1992). The phase of each spectrum is shown next to the spectrum.

band photometry, we obtain an optical luminosity of 3×10^{42} ergs $^{-1}$ for both SNe around maximum. Since SN radiation around maximum is concentrated in the optical, the optical luminosity is a good approximation to the bolometric luminosity. In the case of iPTF14atg, the explosion date is tightly constrained by the SN-companion collision and therefore its rise time to the R -band maximum is 22 days. The total ^{56}Ni mass can be estimated from the peak luminosity and the rise time via the following equation:

$$L_{\text{max}} = \alpha S(t_R), \quad (1)$$

where $S(t_R)$ is the instantaneous radioactive power at the light curve peak that can be expressed as

$$\frac{S(t)}{10^{43} \text{ erg s}^{-1}} = [6.31 \exp(-t/8.8) + 1.43 \exp(-t/111)] \frac{M_{\text{Ni}}}{M_{\odot}}, \quad (2)$$

where t is in units of days. α is an efficiency factor of order unity, depending on the distribution of ^{56}Ni . We adopt a fiducial value of $\alpha = 1.3$ here following Scalzo

et al. (2012). Then we estimate a total ^{56}Ni mass of $0.14 M_{\odot}$ for iPTF14atg.

In contrast, as discussed in §3, iPTF14dpk may experience a “dark” period after the explosion. Therefore its light curve only provides an upper limit on the actual explosion date, or equivalently a lower limit on the rise time, and thus a lower limit of $0.11 M_{\odot}$ on the ^{56}Ni mass.

In addition, we would like to clarify that the main difference of SN2002es-like events from “classical” subluminal SN1991bg-like events is that the former exhibit low velocity absorption features. As shown in Figure 2, around maximum, although the overall spectral shapes look similar among SN2002es-like events and SN1991bg, the velocities of the absorption lines, such as Si II, are obviously lower in SN2002es-like events than in SN1991bg by several thousand km s $^{-1}$. At late time, SN2002es-like events develop multiple narrow features between 5000 Å and 7000 Å while these features are blended in the spectra of SN1991bg-like events (Jha et al. 2006).

3. LIGHT CURVES AT EARLY PHASES

As noted in the previous section, iPTF14atg and iPTF14dpk exhibit different photometric behavior at early phases. In particular, iPTF14atg took more than a week to rise to -17 mag with a mean rise rate of $0.2 \sim 0.3$ mag day $^{-1}$. In contrast, iPTF14dpk shows a steep rise to $r = -16.9$ mag within one day of its last non-detection of $r > -15.1$ mag, indicating an initial rise rate > 1.8 mag day $^{-1}$. In the subsequent epoch, the apparent decline in the iPTF14dpk light curve is not statistically significant.

At first blush, the pre-discovery $5\text{-}\sigma$ upper limits of iPTF14dpk in the magnitude plot may mislead the readers into concluding that the upper limits of iPTF14dpk are roughly consistent with the early νL_{ν} detections of iPTF14atg. However, when plotted in νL_{ν} , the early detections of iPTF14atg are distinct from the non-detections of iPTF14dpk at similar epochs by more than 3σ (see the inset of Figure 1). If we approximate measurement noises with Gaussian distributions, the probability that the iPTF14dpk pre-SN non-detections are consistent with the early-phase detections of iPTF14atg is less than 3×10^{-9} .

3.1. SN-companion interaction

Next, we seek an explanation to the distinct early-phase light curves of the two otherwise similar SNe. Given the spectroscopic typing and almost identical light curves (apart from the early rise), we make a simple and reasonable assumption that *all* SN2002es-like events arise from the same progenitor channel. As noted in Cao et al. (2015), the observed early declining UV pulse from iPTF14atg provides evidence for the SD progenitor channel.

Three energy resources may power the optical light curve of a SN from the SD channel: SN shock breakout, SN-companion collision, and radioactive decay of ^{56}Ni . The shock breakout of a SN Ia lasts for less than a second (Piro et al. 2010), so we do not consider this energy resource to explain the iPTF14atg and iPTF14dpk light curves.

Both the SN-companion-collision powered and radioactively powered components are seen in the light curve of

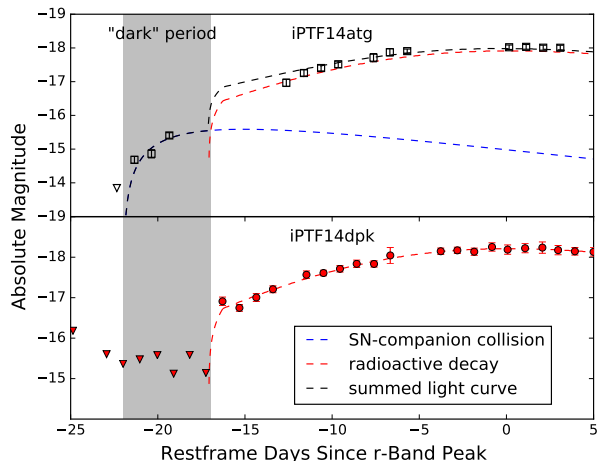


Figure 3. Light curve analysis of iPTF14atg and iPTF14dpk. *Upper panel:* The early R -band light curve of iPTF14atg has two component: the earlier component (blue dashed curve) is the Rayleigh-Jeans tail of the thermal emission computed from SN-companion collision model. The later component (red dashed curve), powered by ^{56}Ni , is represented by the iPTF14dpk light curve offset by 0.1 mag to match the peak magnitude of iPTF14atg. *Lower panel:* The early R -band light curve of iPTF14dpk is purely powered by ^{56}Ni . The post-explosion “dark” period is highlighted in gray.

iPTF14atg. Specifically, its UV/optical light curve before -17 days is dominated by the Rayleigh-Jeans tail of the SN-companion interaction signature, and the light curve after -17 days is mainly from radioactive decay. In order to show this, we fit the SN-companion collision model (Kasen 2010) to its early UV light curve. Noting that a factor of π is missing in the Cao et al. (2015) calculation, we find a good fit with an explosion energy of 3×10^{50} ergs, an ejecta mass of $1.4M_{\odot}$, and a binary separation of $70R_{\odot}$. Then we calculate the R -band light curve from this model and compare it to the observed R -band light curve. As shown in the upper panel of Figure 3, the light curve before -17 days can be entirely attributed to the Rayleigh-Jeans tail emission from the SN-companion collision. In later epochs, radiation from the SN-companion interaction becomes minor and the light curve has to be powered by the radioactive energy.

In fact, as noted by Kasen (2010), given typical mass ratios of a few for SD progenitor binaries of SNe Ia, only less than 10% of the resulting explosions would have geometry that would allow the SN-companion collision signature to be seen by a randomly located observer. For the remaining $> 90\%$ events, we can only see the radioactively powered light curves. This provides a natural explanation to iPTF14dpk: the observed iPTF14dpk light curve is purely powered by its radioactive decay.

If we make a further assumption that both iPTF14atg and iPTF14dpk have similar ejecta structures, then the radioactively powered light curves of iPTF14atg and iPTF14dpk have similar shapes. Despite the observed 0.1 mag difference at peak magnitudes which is probably due to the exact amount of synthesized ^{56}Ni , the light curve of iPTF14atg can be roughly treated as a superposition of the SN-companion collision light curve and the iPTF14dpk light curve (Figure 3).

3.1.1. A Side Note About iPTF14dpk

The sharp rise of iPTF14dpk was initially considered to be a possible SN-companion interaction signature, but our further analysis soon rejected this hypothesis. According to the scaling relations in Kasen (2010), the luminosity from a SN-companion collision $L \propto aE^{7/8}M^{-7/8}$ and the effective temperature $T \propto a^{-1/4}$, where a is the binary separation, E is the explosion energy and M is the total ejecta mass. Since the temperature is very high, the radiation flux in the r band can be approximated by the Rayleigh-Jeans law, i.e., $f_{\nu} \simeq L/(\sigma T^4) \times 2kT\nu^2/c^2 \propto LT^{-3} \propto E^{7/8}M^{-5/8}a^{1/4}$. Hence, the R -band flux is insensitive to the binary separation. If iPTF14dpk has an ejecta mass similar to iPTF14atg, then in order to fit the first detection of $r = -17$ mag of iPTF14dpk, its explosion energy has to be $E \gtrsim 2 \times 10^{51}$ ergs. Such a large explosion energy would then lead to an expansion velocity significantly higher than the low expansion velocity of iPTF14dpk derived from its spectral lines. Furthermore, as the effective temperature remains high, the expansion of the SN would make the R -band flux increase rapidly with time. However, we do not see a fast-rising light curve after the first epoch of iPTF14dpk.

3.2. SN Dark Phase

Given a binary separation of $70R_{\odot}$ and an ejecta velocity of $5 \times 10^3 \text{ km s}^{-1}$, the SN ejecta of iPTF14atg hit its companion star within three hours of SN explosion. Here the SN-companion signature provides an accurate approximation to the explosion date for iPTF14atg, i.e., at -22.1 days. Given the similarity between iPTF14atg and iPTF14dpk, it is reasonable to assume that the rise time of iPTF14dpk is similar to that of iPTF14atg. Under this framework we explore the physical consequences below.

As shown in the lower panel of Figure 3, the radioactively powered light curve of iPTF14dpk was not visible until -16 days. This soon leads to an interesting result that iPTF14dpk had a “dark” period between its explosion and the first light of its radioactively powered light curve. In our framework, this “dark” period also existed in iPTF14atg, but was lighted by the SN-companion interaction signature. If iPTF14atg had been observed in a different viewing angle, then the SN-companion interaction signature would become invisible and hence the “dark” period would appear.

The “dark” period is essentially the timescale for the radioactive decay energy to reach the SN photosphere. During the expansion of the SN ejecta, in the Lagrangian point of view, the photosphere moves inwards while the energy diffusive front from the shallowest layer of ^{56}Ni moves outwards. As shown in a toy model in Figure 4, a deep deposition of ^{56}Ni will delay the first light of a SN by a few days, compared to a shallow deposition.

A “dark” phase has also been suggested in the normal Type Ia SN2011fe (Hachinger et al. 2013; Piro & Nakar 2014). Very recently, Piro & Morozova (2015) performed similar but more sophisticated calculations on the durations of the “dark” period for normal Type Ia SNe with different ^{56}Ni depositions. They used more realistic WD models from MESA (Paxton et al. 2011), added ^{56}Ni at different deposition depths, and performed radiative transfer calculations with SNEC (Morozova et al. 2015).

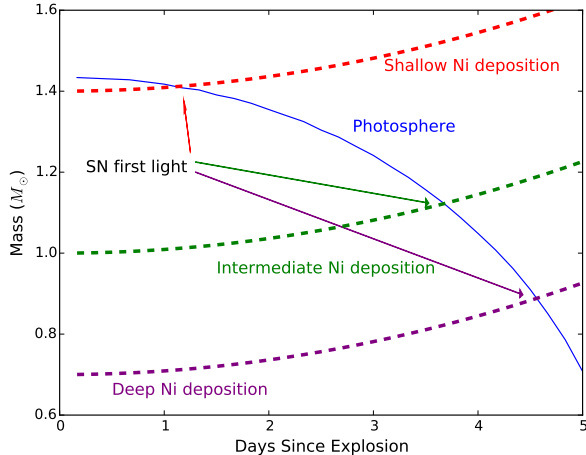


Figure 4. Locations of photosphere and diffusive fronts as a function of time since explosion. The y -axis is the mass coordinate of the SN ejecta. The location of photosphere (blue solid curve) is calculated for a $1.44M_{\odot}$ white dwarf model with a constant opacity $0.2 \text{ cm}^2 \text{ g}^{-1}$ and a SN expansion velocity 10^5 km s^{-1} . The dashed red, green and purple curves correspond to diffusive wavefronts for the shallowest ^{56}Ni layer located at $1.4M_{\odot}$, $1.0M_{\odot}$ and $0.7M_{\odot}$. The propagation of the diffusive wavefront is approximated by $\Delta M \propto t^2$. The intersection points between the solid curve and the dash curves represent the time of SN first light.

They found that deep deposition of ^{56}Ni in a normal Type Ia SN may lead to a “dark” period of a couple of days.

4. DISCUSSION AND CONCLUSION

In this letter, we present optical observations of two low-velocity Type Ia supernovae, iPTF14atg and iPTF14dpk, from the intermediate Palomar Transient Factory. Both are photometrically and spectroscopically similar to the prototypical SN2002es (Ganeshalingam et al. 2012). Despite their similarities around and after maximum, we observed different initial rise behaviors in these two events. While iPTF14atg experiences a steady and slow rise which lasts for 22 days, iPTF14dpk shows a sharp initial rise to -16.9 mag within a day of discovery and then joins the rise behavior of iPTF14atg. The apparent rise time of iPTF14dpk is only 16 days.

Based on the spectroscopic typing and similar photometric evolution, and based on the observed early declining ultraviolet pulse in iPTF14atg (Cao et al. 2015), we make a reasonable assumption that all SN2002es-like events arise from the single-degenerate progenitor channel. By analyzing the early R -band light curves of iPTF14atg and iPTF14dpk, we show that:

- The light curve of iPTF14atg can be decomposed into the early SN-companion interaction component and the late radioactively powered component. The latter component resembles the full light curve of iPTF14dpk. The absence of the early component in iPTF14dpk is due to an unfavorable viewing angle along which the SN-companion interaction is blocked by the optically thick ejecta.
- An SN2002es-like event, or for that matter any Type Ia supernova in general (Hachinger et al. 2013; Piro & Nakar 2014), may experience a “dark”

phase between the actual explosion and the first light of its radioactively powered light curve. The duration of the “dark” phase is the timescale for the radioactive decay energy to reach the SN photosphere.

- In the case of iPTF14atg, the “dark” phase was lighted by Rayleigh-Jeans emission from the SN-companion collision.

Moving forward, collecting a large sample of young SN2002es-like light curves will be valuable to verify the viewing geometry effect as well as the “dark” periods. This sample will also put constraints on the geometry of the progenitor binaries for SN2002es-like events and thus the mass ratio. For example, if the mass ratio between the donor and the primary white dwarf is one, then we would have to find 14 young SN2002es-like events, before we could observe the SN-companion interaction again.

The upcoming Zwicky Transient Facility (ZTF; Smith et al. 2014) and the planned wide-field fast-cadence ultraviolet surveys, such as ULTRASAT (Sagiv et al. 2014), will provide opportunities to collect the sample in both the optical and ultraviolet, respectively. Assuming that the SN2002es-like event rate is about 10% of the normal Type Ia supernova rate, we estimate that ZTF will discover eight young SN2002es-like events every year and that ULTRASAT will find one dozen in its two-year mission lifetime. These two projects, together with other ongoing and planned fast-cadence surveys, will provide a big sample to estimate the observational occurrence of the SN-companion interaction and therefore to put constraints on the geometry of the progenitor binaries. Additionally, since the presence of a companion star in a SN explosion adds asphericity of the SN ejecta, spectropolarimetric follow-up observations of SN2002es-like supernovae will also provide independent constraints on the viewing angles (Kasen et al. 2004).

YC and PEN acknowledge support from the DOE under grant DE-AC02-05CH11231, Analytical Modeling for Extreme-Scale Computing Environments. YC also acknowledges support from the National Science Foundation PIRE program grant 1545949. AG is supported by the EU/FP7 via ERC grant no. 307260, the Quantum Universe I-Core programme by the Israeli Committee for Planning and Budgeting and the ISF; by Minerva and ISF grants; by the Weizmann-UK ‘making connections’ programme; and by Kimmel and ARCHES awards.

This research used resources of the National Energy Research Scientific Computing Center, a DOE Office of Science User Facility supported by the Office of Science of the U.S. Department of Energy under Contract No. DE-AC02-05CH11231. Part of this research was carried out at the Jet Propulsion Laboratory, California Institute of Technology, under a contract with the National Aeronautics and Space Administration.

REFERENCES

- Cao, Y., Kulkarni, S. R., Howell, D. A., et al. 2015, *Nature*, 521, 328
 Filippenko, A. V., Richmond, M. W., Branch, D., et al. 1992, *AJ*, 104, 1543

- Fink, M., Kromer, M., Seitenzahl, I. R., et al. 2014, MNRAS, 438, 1762
- Fitzpatrick, E. L. 1999, PASP, 111, 63
- Foley, R. J., McCully, C., Jha, S. W., et al. 2014, ApJ, 792, 29
- Foley, R. J., Challis, P. J., Chornock, R., et al. 2013, ApJ, 767, 57
- Ganeshalingam, M., Li, W., Filippenko, A. V., et al. 2012, ApJ, 751, 142
- Hachinger, S., Mazzali, P. A., Sullivan, M., et al. 2013, MNRAS, 429, 2228
- Jha, S., Branch, D., Chornock, R., et al. 2006, AJ, 132, 189
- Kasen, D. 2010, ApJ, 708, 1025
- Kasen, D., Nugent, P., Thomas, R. C., & Wang, L. 2004, ApJ, 610, 876
- Law, N. M., Kulkarni, S. R., Dekany, R. G., et al. 2009, PASP, 121, 1395
- Maoz, D., Mannucci, F., & Nelemans, G. 2014, ARA&A, 52, 107
- McCully, C., Jha, S. W., Foley, R. J., et al. 2014, Nature, 512, 54
- Morozova, V., Piro, A. L., Renzo, M., et al. 2015, ApJ, 814, 63
- Ofek, E. O., Laher, R., Law, N., et al. 2012a, PASP, 124, 62
- Ofek, E. O., Laher, R., Surace, J., et al. 2012b, PASP, 124, 854
- Oke, J. B., & Gunn, J. E. 1982, PASP, 94, 586
- Oke, J. B., Cohen, J. G., Carr, M., et al. 1995, PASP, 107, 375
- Paxton, B., Bildsten, L., Dotter, A., et al. 2011, ApJS, 192, 3
- Piro, A. L., Chang, P., & Weinberg, N. N. 2010, ApJ, 708, 598
- Piro, A. L., & Morozova, V. S. 2015, ArXiv e-prints, arXiv:1512.03442
- Piro, A. L., & Nakar, E. 2014, ApJ, 784, 85
- Planck Collaboration, Ade, P. A. R., Aghanim, N., et al. 2014, A&A, 571, A16
- Poznanski, D., Prochaska, J. X., & Bloom, J. S. 2012, MNRAS, 426, 1465
- Rau, A., Kulkarni, S. R., Law, N. M., et al. 2009, PASP, 121, 1334
- Sagiv, I., Gal-Yam, A., Ofek, E. O., et al. 2014, AJ, 147, 79
- Scalzo, R., Aldering, G., Antilogus, P., et al. 2012, ApJ, 757, 12
- Schlafly, E. F., & Finkbeiner, D. P. 2011, ApJ, 737, 103
- Smith, R. M., Dekany, R. G., Bebek, C., et al. 2014, in Society of Photo-Optical Instrumentation Engineers (SPIE) Conference Series, Vol. 9147, Society of Photo-Optical Instrumentation Engineers (SPIE) Conference Series, 79
- White, C. J., Kasliwal, M. M., Nugent, P. E., et al. 2015, ApJ, 799, 52
- Yaron, O., & Gal-Yam, A. 2012, PASP, 124, 668